On the Annual Cycle in the Tropical Eastern Central Pacific

BIN WANG

Department of Meteorology, School of Ocean and Earth Science and Technology, University of Hawaii, Honolulu, Hawaii

(Manuscript received 16 March 1992, in final form 31 January 1994)

ABSTRACT

In the tropical eastern central Pacific Ocean, the annual cycle in sea surface temperature (SST), surface winds and pressure, and clouds are alternatively dominated by an antisymmetric (with respect to the equator) monsoonal mode in February and August and a quasi-symmetric equatorial–coastal mode in May and November, both having a period of one year. The monsoonal mode is forced by the differential insolation between the Northern and Southern Hemispheres. The surface wind variation of the monsoonal mode tends to lead SST variation in late spring/fall. The equatorial–coastal mode originates from atmosphere–ocean interaction. Its development is characterized by contemporaneous intensification and spatial expansion (westward and poleward phase propagation).

The interaction between the forced monsoonal mode and the coupled equatorial–coastal mode plays a critical role in the annual cycle. From October to February, the decline of the southern winter regime of the monsoonal mode initiates and sustains the amplification of the equatorial–coastal mode, causing annual weakening of the cold tongue. From April to June, the enhancement of the poleward SST gradient associated with the decay of the equatorial–coastal mode initiates the eastern North Pacific summer monsoon. Atmosphere–ocean interaction is directly responsible for the annual weakening and reestablishment of the cold tongue, whereas the annual cycle in insolation regulates the interaction indirectly through the forced monsoonal mode.

1. Introduction

The solar radiation flux at the surface under clear skies can be decomposed into a symmetric and an antisymmetric component with respect to the equator as shown in Fig. 1. The antisymmetric component represents the contrast in insolation between the Northern and Southern Hemispheres and is forced by the annual cycle in solar declination angle. The symmetric component, on the other hand, is caused by the semiannual cycle in solar declination (maximized on the equator at equinoxes) and the annual cycle in the sun–earth distance (maximum in northern winter solstice when the earth is closest to the sun and minimum in northern summer solstice). In the vicinity of the equator the amplitude of the semiannual harmonic is about 50% larger than that of the annual harmonic. Away from the equatorial regions, however, the antisymmetric annual harmonic dominates (Fig. 1).

The atmospheric response to the insolational forcing is strikingly different over the Eastern and Western Hemisphere oceans. Regardless of the dominant semiannual variation of solar radiation in the equatorial region, SST and clouds in the equatorial eastern Pacific, as well as in the Atlantic, have a dominant annual cycle with a warm and wet season occurring in boreal spring and a cold and dry season in boreal fall (Wyrtki 1965; Hastenrath and Lamb 1978; Horel 1982; Mitchell and Wallace 1992). Why does the periodicity of annual variation there differ from that of insolational forcing? How does the solar radiational forcing affect the annual variation in that region? What roles do the oceanic processes interacting with the atmosphere play?

This paper presents an observational analysis of the peculiar annual cycle in the tropical eastern central Pacific and explores its physical causes, in particular, the causes responsible for annual weakening and reestablishment of the equatorial cold tongue and the onset of the eastern North Pacific monsoon. There are a number of papers [for a brief review refer to Horel (1982) and Mitchell and Wallace (1992)] and several comprehensive atlases (e.g., Wyrtki and Meyers 1975; Hastenrath and Lamb 1977; Weare et al. 1980; Janowiak et al. 1985; Sadler et al. 1987) that document the annual variation of SST and atmospheric variables in the tropical Pacific by describing features of the climatological monthly means. The present analysis focuses on the departure of climatological monthly mean from the long-term mean condition (the annual mean), which will be termed as *annual perturbation* in this paper. The analysis of the annual perturbations will provide additional understanding of the nature of the interaction between solar radiational forcing and atmosphere–ocean coupling in the annual cycle of the equatorial Pacific cold tongue.

Corresponding author address: Dr. Bin Wang, Dept. of Meteorology, School of Ocean and Earth Science and Technology, University of Hawaii at Manoa, 2525 Correa Road, Honolulu, HI 96822.

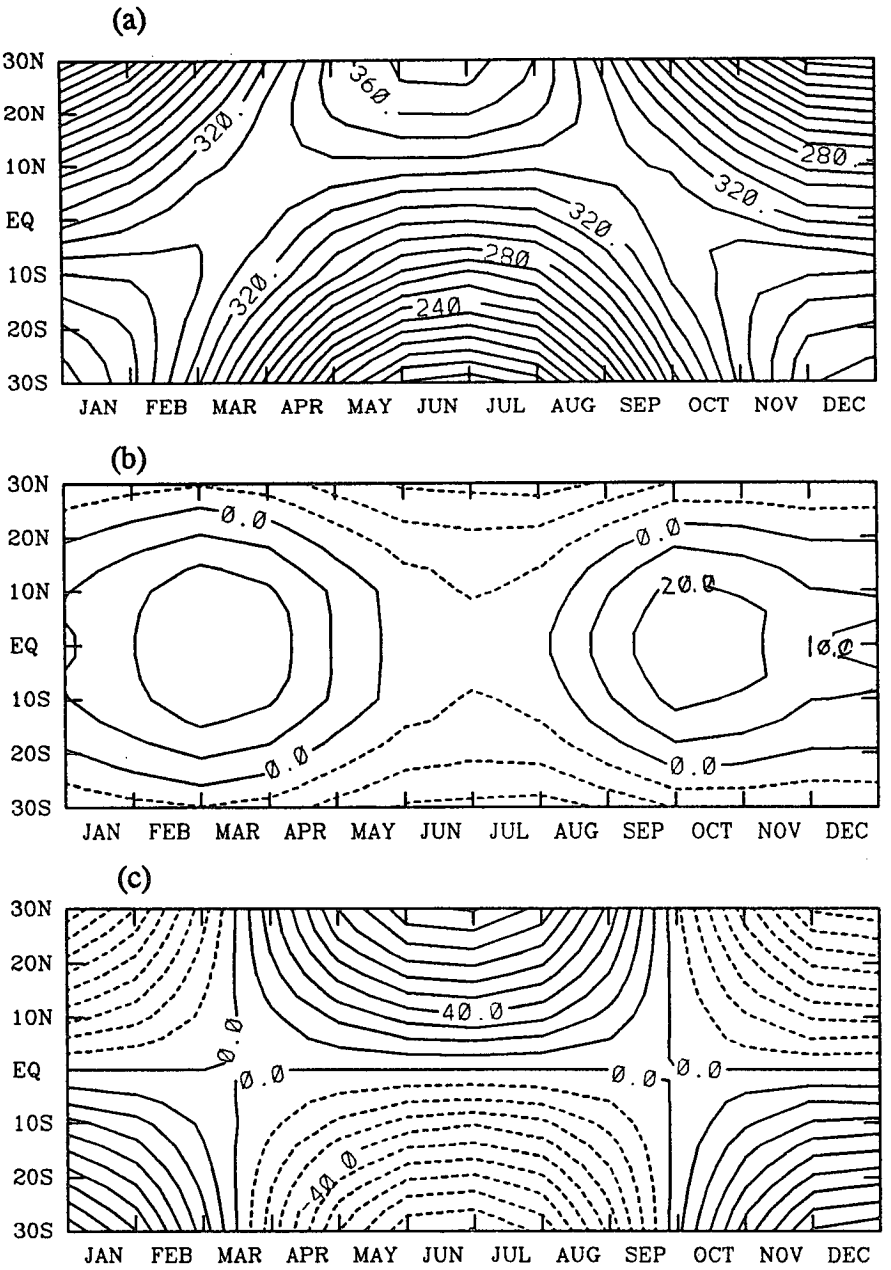

FIG. 1. The net shortwave radiation flux (W m^{-2}) at the surface under clear skies (a) and its symmetric (b) and antisymmetric (c) component after removing the areal mean (307.2 W m^{-2}). The data in (a) is adopted from Budyko and Miller (1974).

Section 2 describes data, and section 3 brief characteristics of the background mean state. Section 4 describes analysis procedure, beginning by showing that the annual perturbations of SST and surface winds in the eastern central Pacific are alternatively dictated by a symmetric and an antisymmetric component during the course of the year. To explore the origin and evolution of these components, the annual perturbation was further partitioned into two orthogonal modes: a quasi-symmetric, equatorial–coastal mode and an antisymmetric, monsoonal mode. The spatiotemporal structures and the origin of the two modes are investigated in sections 5 and 6, respectively. The results indicate that the monsoonal mode originates from the insolational contrast between the Northern and Southern Hemispheres, whereas the equatorial–coastal mode is a result of ocean–atmosphere–land interaction. The causes of the weakening and reestablishment of the

cold tongue are examined in section 7. It is demonstrated that the interaction between the forced monsoonal mode and the coupled equatorial–coastal mode plays a critical role in the annual cycle of the cold tongue and eastern North Pacific monsoon. The last section summarizes major findings and discusses the limitations of the analysis and issues that require further investigations.

2. Data

Climatological monthly means of SST, sea level pressure (SLP), surface winds, outgoing longwave radiation (OLR), and frequency of highly reflective cloud (HRC) are used in the present analysis. The climatological monthly mean SST, SLP, and surface winds were computed by Sadler et al. (1987) using the Comprehensive Ocean–Atmosphere Data Set (COADS) for the period from 1900 to 1979. The averaged values of these variables are available for 2° latitude–longitude boxes between 30°S and 40°N. Outgoing longwave radiation data were derived from polar-orbiting satellites. The procedure used to derive these data was described by Gruber and Krueger (1984). The climatological monthly means of OLR were computed on a 2.5° × 2.5° grid using the data from June 1974 to December 1989 with one gap of 10 months in 1978. The OLR is used as an indirect measurement for deep convection. Its fluctuations over the cold tongue, however, often reflect changes in the amount of stratocumulus clouds. In the northeast Pacific OLR is also not a reliable estimate for deep convection because of the contamination by cirrus clouds (Morrissey 1986). For this reason, HRC data derived from subjective analysis of visible and infrared satellite images (Garcia 1985) are also used to infer deep convection. Climatological monthly mean frequency of HRC was computed for 1° latitude–longitude boxes between 25°N and 25°S using the data from January 1971 to July 1987. The analysis domain is confined to the region between 20° latitude south and north of the equator and between 80°W and the date line (Fig. 2b). To reduce the amount of computation for empirical orthogonal function (EOF) analysis, climatological monthly means were computed for 4° latitude by 10° longitude squares.

3. Background mean states

Because the annual perturbations occur in an inhomogeneous (spatially varying) annual mean state, it is worthwhile to briefly review the features of the annual mean state. The tropical eastern and central Pacific is characterized by the presence of an equatorial–coastal cold SST tongue (Fig. 2a) that is well known for its prominent interannual variability. The El Niño manifests itself as a weakening or disappearance of the cold tongue. The cold tongue also exhibits pronounced annual variation. In fact, its horizontal extent can be well outlined by the area in which annual range of SST is relatively large (Fig. 2b). Within the immense domain of the cold tongue, the *annual warming* (defined as the transition from below to above the annual mean SST) displays a distinct *northwestward* phase propagation (Fig. 2c). The annual extreme warm phase exhibits a similar northwestward propagation (Wyrtki 1965). Over the cold tongue prevail divergent southeast trades. The zero-divergence contour nearly coincides with the periphery of the cold tongue (Fig. 2b). The descending motion accompanying the divergent trades maintains trade inversions that, in turn, restrain convective development and stabilize trade wind systems. The steady easterly trades build up east–west slope of the thermocline, rendering the eastern Pacific subject to the influence of upwelling and entrainment. The dynamic processes (upwelling and advection by currents) play an essential part in the maintenance of the cold tongue (Wyrtki 1981).

4. Analysis methods

a. Partition of annual perturbation

Inspection of Fig. 3 reveals that the annual perturbations in SST and surface winds are alternatively dominated by two regimes. The May–November pattern is somewhat symmetric, whereas the February–August pattern tends to be antisymmetric with respect to the equator in SST and zonal wind. To examine detailed evolution of each regime and to determine their nature, the annual perturbation was partitioned into a symmetric (denoted by subscript s) and an antisymmetric component (denoted by subscript a) defined by

$$F_s(x, y) = [F(x, y) + F(x, -y)]/2, \quad (1a)$$

$$F_a(x, y) = [F(x, y) - F(x, -y)]/2, \quad (1b)$$

where $F(x, y)$ represents an annual perturbation of any variable at a given month of the year; x and y are longitudinal and latitudinal distance ($y = 0$ at the equator), respectively.

It can be shown that F_s and F_a are orthogonal in the sense that the total variance of F equals the sum of the variances of F_s and F_a. The symmetric and antisymmetric components of the partial derivatives of F can be expressed by the partial derivatives of F_s and F_a:

$$(\partial F/\partial x)_s = \partial F_s/\partial x, \quad (\partial F/\partial x)_a = \partial F_a/\partial x, \quad (2a)$$

$$(\partial F/\partial y)_s = \partial F_a/\partial y, \quad (\partial F/\partial y)_a = \partial F_s/\partial y. \quad (2b)$$

Thus, separation of the continuity equation in pressure coordinates into symmetric and antisymmetric parts yields

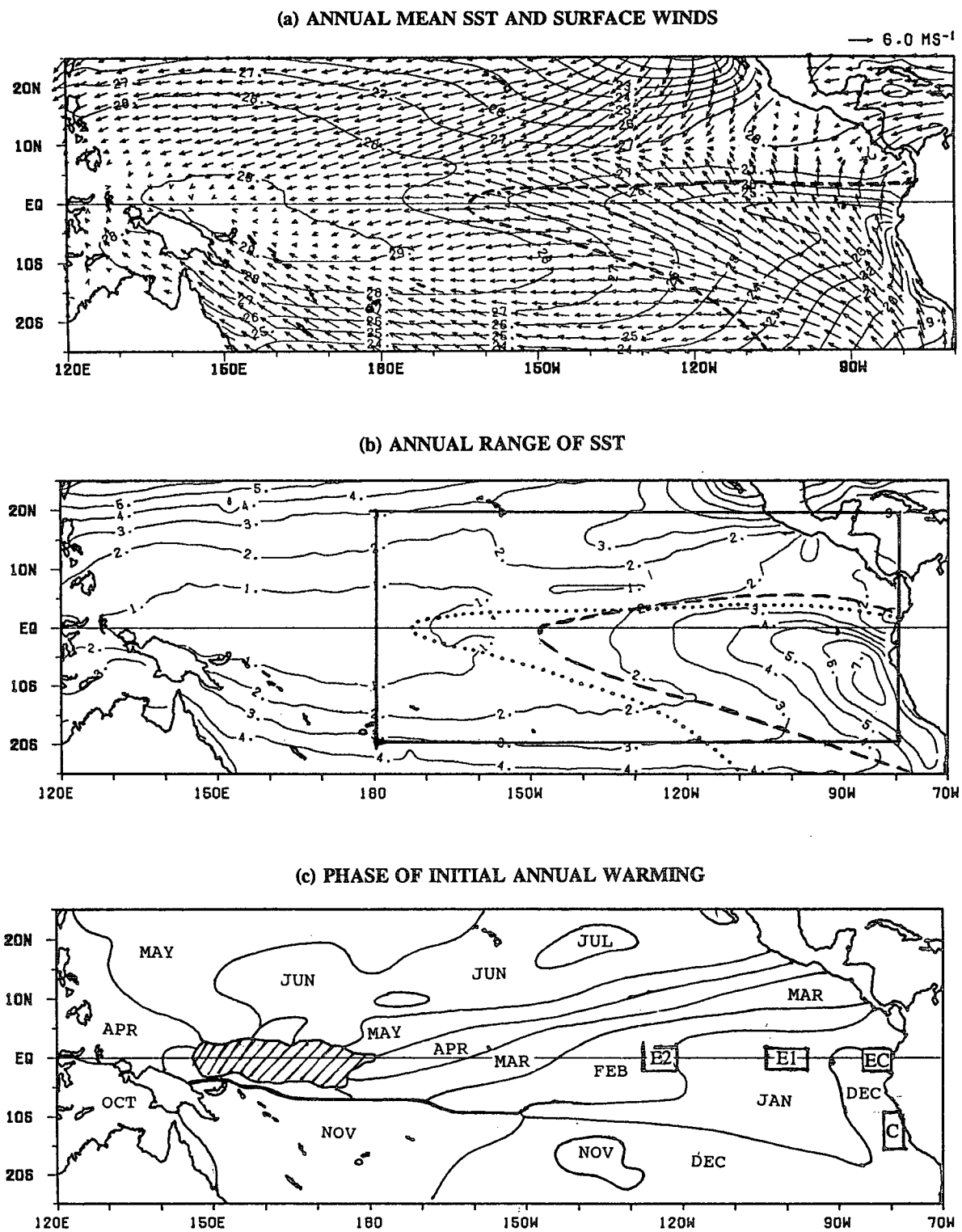

FIG. 2. (a) Annual-mean SST (contours) and surface winds (arrows). The heavy dashed line encloses the equatorial cold tongue in which SST is lower than its zonally averaged value over the global oceans as defined by Bjerknes (1969). (b) Annual range of SST. The heavy dashed line outlines the area in which annual range of SST is relatively large. The heavy dotted line is the contour of zero surface wind divergence. The heavy solid lines indicate the boundaries of the analysis domain. (c) Phase of the annual warming. Phase is not shown for the area where the annual range of SST is less than 0.5°C. The boxes C, E1, E2, and EC indicate the four selected locations used in Table 3.

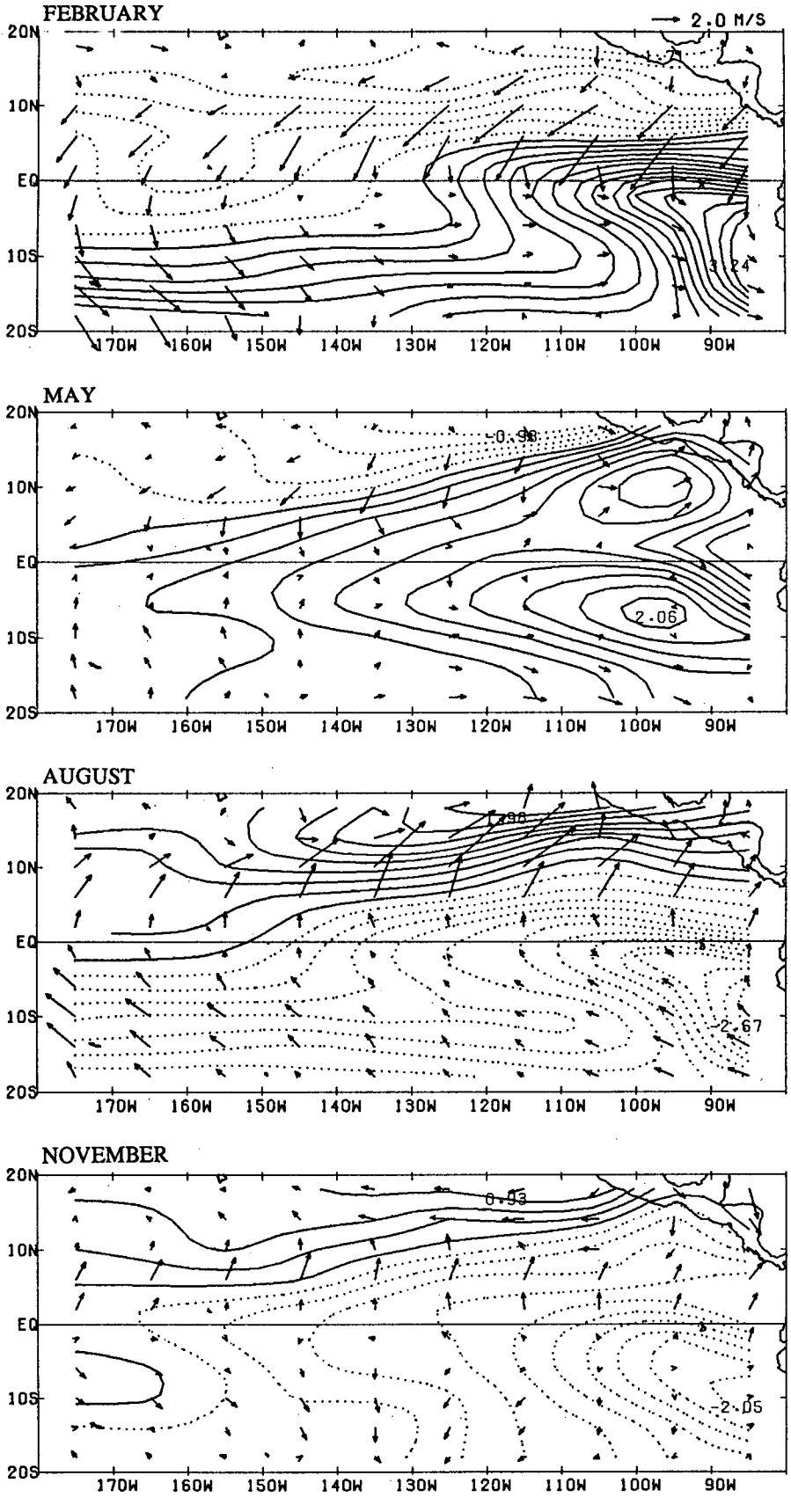

FIG. 3. Climatological monthly mean departure (with respect to the annual mean) of SST and surface winds (arrows) for February, May, August, and November. The solid (dotted) contours represent positive (negative) SST starting from 0.1°C with an interval of 0.2°C.

TABLE 1. Mean variance of SST (T) (deg^2) averaged over the analysis domain (20°–20°N, 180°–80°W) and the percentile of variances for its symmetric (T_s) and antisymmetric (T_a) components.

	Jan	Feb	Mar	Apr	May	Jun	Jul	Aug	Sep	Oct	Nov	Dec
T	53	120	163	157	69	19	39	106	139	124	52	25
T_s	26	27	42	61	80	86	25	29	33	42	65	91
T_a	74	73	58	39	20	14	75	71	67	58	35	9

$$\frac{\partial u_s}{\partial x} + \frac{\partial v_a}{\partial y} + \frac{\partial \omega_s}{\partial p} = 0 \tag{3}$$

and

$$\frac{\partial u_a}{\partial x} + \frac{\partial v_s}{\partial y} + \frac{\partial \omega_a}{\partial p} = 0. \tag{4}$$

Equations (3) and (4) indicate that for a given wind field, mass conservation requires the antisymmetric (symmetric) meridional wind be always linked to the symmetric (antisymmetric) zonal wind. This linkage is consistent with the two observed regimes shown in Fig. 3. In this paper, a *symmetric wind field* will be referred to as the one that consists of a symmetric component of zonal wind and an antisymmetric component of meridional wind. Likewise, an *antisymmetric wind field* is meant to be composed of antisymmetric zonal and symmetric meridional winds.

Table 1 shows that in the tropical eastern central Pacific the peaks of variance in SST occur in equinoctial seasons (March–April and September–October). The variances carried by the symmetric and antisymmetric components are comparable. The fractional variances accounted for by the two components, however, are out of phase. In January–March and July–October, the antisymmetric component is more prominent, whereas in April–June and November–December, the symmetric component dominates. These conclusions are also valid for SLP, surface winds, and OLR (tables not shown).

All antisymmetric fields examined here show large meridional gradients and small zonal gradients. In addition, the zonal variation is primarily confined to the east of 105°W (figure not shown). This implies that a zonal-mean antisymmetric component defined by

$$\overline{F_a}(y) = \frac{1}{x_2 - x_1} \int_{x_1}^{x_2} F_a(x, y)\, dx \tag{5}$$

can well represent the antisymmetric field over the open ocean, whereas the departure of the antisymmetric component from its zonal mean

$$F_a' \equiv F_a - \overline{F_a}, \tag{6}$$

depicts, to a large extent, the variations originating from the coastal or continental effects. In (5), x_1 and x_2 represent the date line and 80°W, respectively.

The maintenance of the equatorial Pacific cold tongue involves both equatorial and coastal upwelling as well as advection by ocean currents. Analysis of the symmetric component in isolation may obscure the linkage between the equatorial and coastal processes. For this reason, a quantity that includes both symmetric component and the zonal departure of the antisymmetric component is further defined as

$$E(x, y) = F_s(x, y) + F_a'(x, y), \tag{7}$$

which is referred to as an equatorial–coastal component. It can be shown that the zonal-mean antisymmetric and the equatorial–coastal components are orthogonal in terms of variance decomposition.

b. *Multivariate extended EOF analysis*

In order to detect possible coherent annual variation between oceanic and atmospheric fields, multivariate extended EOF (MV-EEOF) analysis was applied to the equatorial–coastal components of SST, SLP, surface winds, and OLR. A concise discussion of the multivariate EOF is found in Wang (1992). In view of the cyclic nature of the annual variation, extended EOF (EEOF) is adopted to derive variation patterns of dominant sequences of events. Detailed description of the EEOF was given by Weare and Nasstrom (1982). By considering spatial and temporal correlations as well as the correlations among different variables, the MV-EEOF analysis provides a powerful tool to compact large datasets and to reveal possible coherent variability of the atmosphere–ocean system.

5. Coupled equatorial–coastal mode

This section describes the coherent annual variation of the equatorial–coastal components in SST, SLP, surface winds, and OLR (for simplicity, hereafter referred to as an *equatorial–coastal mode*), which depicts the annual cycle of the equatorial cold tongue.

The two most important eigenvectors of the equatorial–coastal mode, E1 and E2, explain, respectively, 52% and 30% of the total variance of all five fields. The SST, SLP, and meridional wind fields have greater than average variance contribution to the total variance carried by E1 and E2 (Table 2).

Figure 4 presents the spatial patterns of SST and surface winds for E1 and E2 for the sequences t,

TABLE 2. Percentile of variances for each field carried by E1 and E2 of MV-EEOF analysis of the equatorial–coastal mode: P_s, u_s, and v_s denote sea level pressure, surface zonal wind, and meridional wind, respectively.

	SST	P_s	v_s	OLR	u_s	Mean
E1	0.55	0.54	0.54	0.49	0.47	0.52
E2	0.39	0.32	0.30	0.26	0.24	0.30
E1 + E2	0.94	0.86	0.84	0.75	0.72	0.82

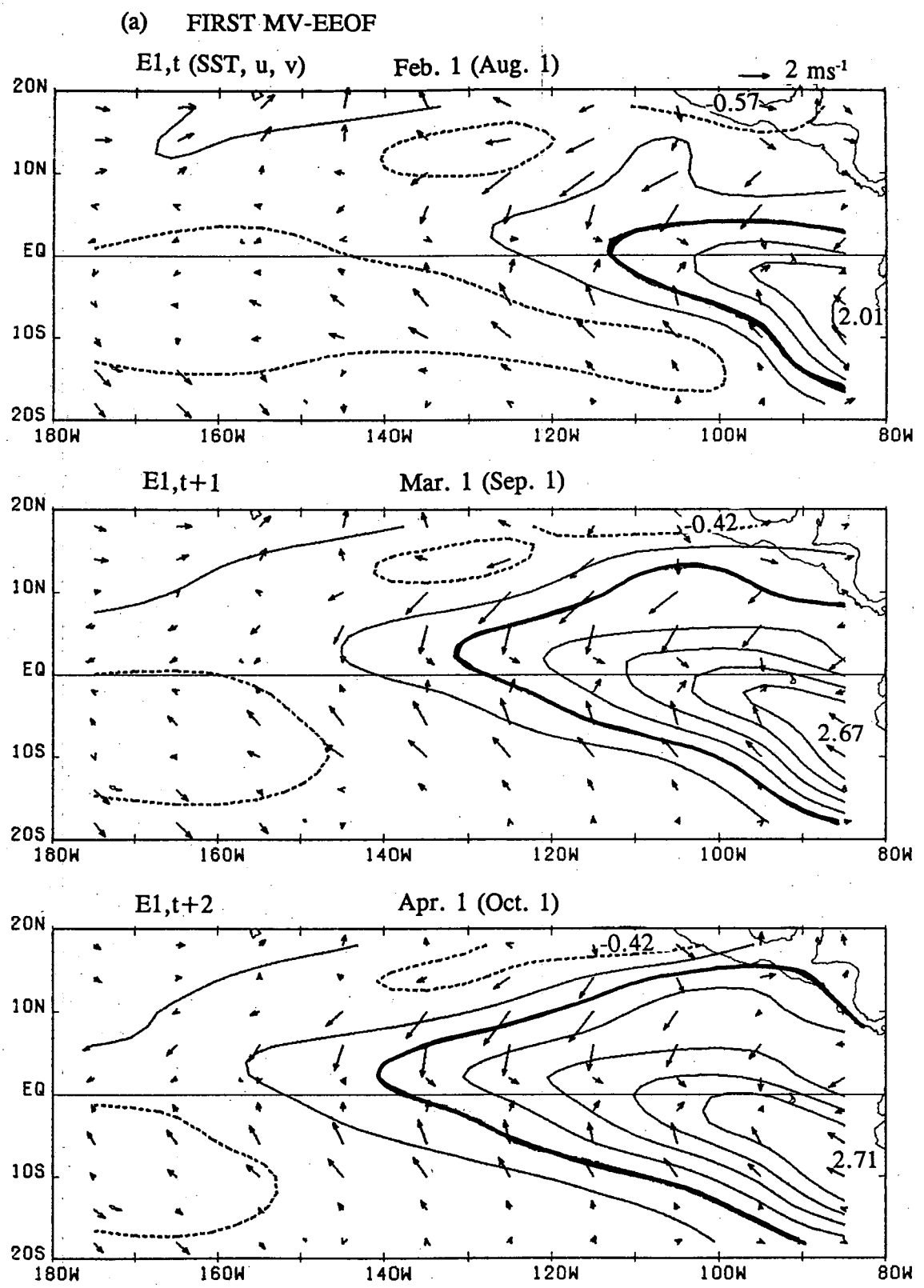

FIG. 4. (a) The first multivariate extended EOF (MV-EEOF) of the equatorial mode for SST (contour interval is 0.4°C) and surface winds at time t, $t + 1$, and $t + 2$ months. The isotherm of 0.6°C is marked by heavy lines. For more explanations

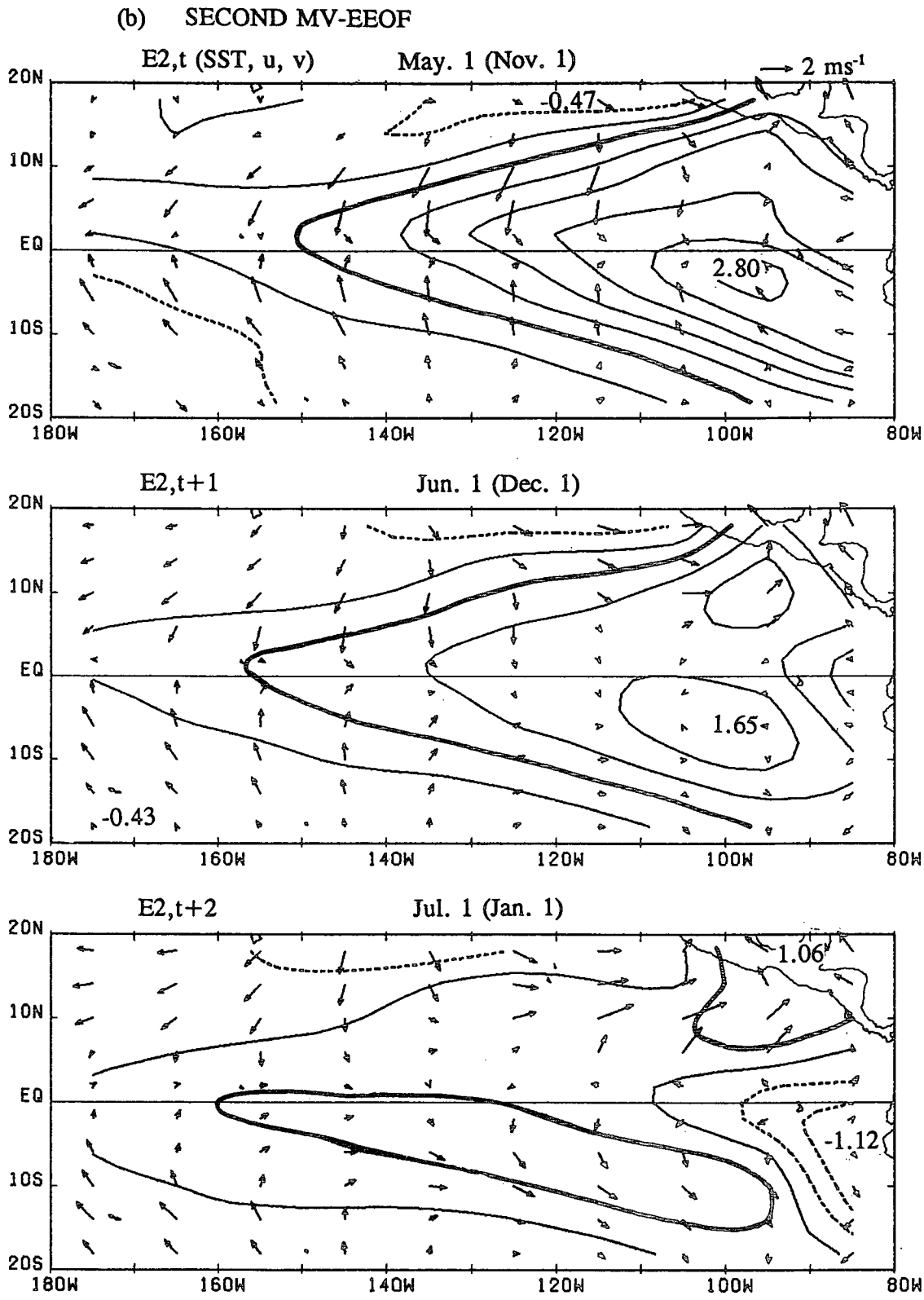

FIG. 4. (*Continued*) see section 3. (b) As in (a) except for the second MV-EEOF.

$t + 1$, $t + 2$ months. Figure 5 shows the principal components, $C_1(t)$ and $C_2(t)$, associated with E1 and E2, respectively. The sum C_1E1 + C_2E2 is used to describe the annual cycle of the equatorial–coastal mode. Because $C_2(t)$ vanishes between January and February, the three panels in Fig. 4a may be viewed as the spatial patterns on 1 February, 1 March, and 1 April, respectively. The E1 patterns with negative polarities at t, $t + 1$, and $t + 2$ represent the fields on 1 August, 1 September, and 1 October, respectively. Similarly, E2, t, E2, $t + 1$, and E2, $t + 2$ shown in Fig. 4b can be interpreted as the fields on 1 May, 1 June, and 1 July, whereas their counterparts with opposite polarities represent the fields on 1 November, 1 December, and 1 January, respectively.

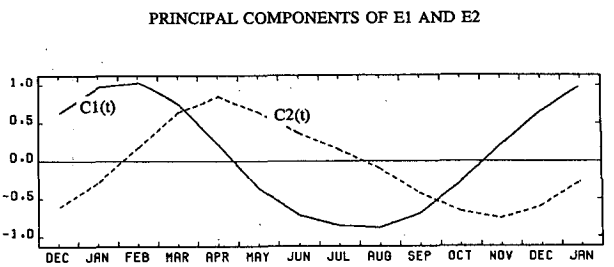

FIG. 5. The principal components associated with the first [C1(t)] and second [C2(t)] MV-EEOF.

a. *Evolution of the equatorial–coastal mode*

The annual warming is characterized by simultaneous expansion in the warming area and increase in overall and maximum intensities. The warming first occurs off the coast of South America, and on 1 January the area where temperature is more than 0.6°C higher than the annual mean is located east of 90°W (the opposite polarity of E2, $t + 2$ in Fig. 4b). It then extends westward and poleward, and by 1 May the contour of 0.6°C reaches 16°N, 150°W. The mean zonal speed of the westward extension along the equator signified by the 0.6°C isotherm is about 16° longitude per month (0.68 m s^{-1}) from 1 January to 1 May. The northward extension is most evident along 95°W, with a mean speed of about 4° latitude per month. Accompanying the expansion of warming area, the maximum warming increases from 1.1°C on 1 January to 2.8°C on 1 May. Note that while the warming area expands continuously, the center of warming tends to stay where the annual range of SST is maximum (8°S, 85°W) and where the thermocline is shallowest (4°S, 95°W) (Meyers 1979).

During May and June the size of the warm (higher than annual mean) area changes little, but the overall intensity decreases continuously (Fig. 4b). The center of the warm area splits into two, moving poleward in respective hemispheres. East of 110°W the rapid decrease of SST along the equator and the poleward propagation of the warm center transform the warm area from a triangle to a V shape. This structural change in warm area implies an enhancement of SST gradients north of the cold tongue that favors the onset of the eastern North Pacific summer monsoon. This will be further discussed in section 7.

The cooling (defined as the transition from above to below annual mean) starts sometime in June off the coast of Peru and Ecuador. The evolution of the cooling is basically a mirror image of that of warming except with a slightly reduced amplitude (Fig. 5).

The MV-EEOF analysis of the equatorial mode reveals a poleward propagation of warm area along 95°W. This is possibly due to the suppressed poleward Ekman transport of upwelled cool water and the westward dispersion of coastal warming by Rossby waves. The pronounced northward propagation in the Northern Hemisphere is also partially ascribed to the annual march in insolation and the effect of land heating over Mexico.

b. *Coherent structure of the equatorial–coastal mode*

In the developing phase (approximately 1 April), Fig. 4a (E1, $t + 2$) and Figs. 6a and 6b show that the SLP perturbation of the equatorial–coastal mode tends to have the opposite sign as that of SST perturbation. This indicates that the boundary layer air temperature and density are modified by SST through surface buoyancy fluxes, so that the pressure perturbation induced by the density perturbation is negatively correlated with the SST perturbation (Lindzen and Nigam 1987). The surface wind perturbation can be understood in terms of three-force (the Coriolis force, friction, and pressure gradient force) balance in the boundary layer. In the vicinity of the equator between about 3°N and 3°S, the pressure gradient force is primarily balanced by friction; thus, winds are zonal, blowing down pressure gradient. Outside the narrow equatorial zone the divergence is primarily due to the meridional derivative of the meridional wind component. The divergence perturbation is, therefore, quasi-symmetric about the equator. The negative OLR coincides roughly with surface convergence (Fig. 6). Note that along the equator the negative OLR and convergence are also nearly in phase with the perturbation westerlies. They propagate together westward and lead the positive SST perturbation by about a quarter of cycle. These structural characteristics are essentially the same as those of the ENSO anomaly in the eastern Pacific as documented by Wang (1992).

The structure of the SLP and surface winds suggests that the atmospheric perturbation is forced by SST perturbation. On the other hand, the westward propagation of the SST perturbation indicates a feedback of wind stress to the ocean, which promotes the westward propagation of warming by enhancing downwelling to the west of the maximum SST (Bjerknes

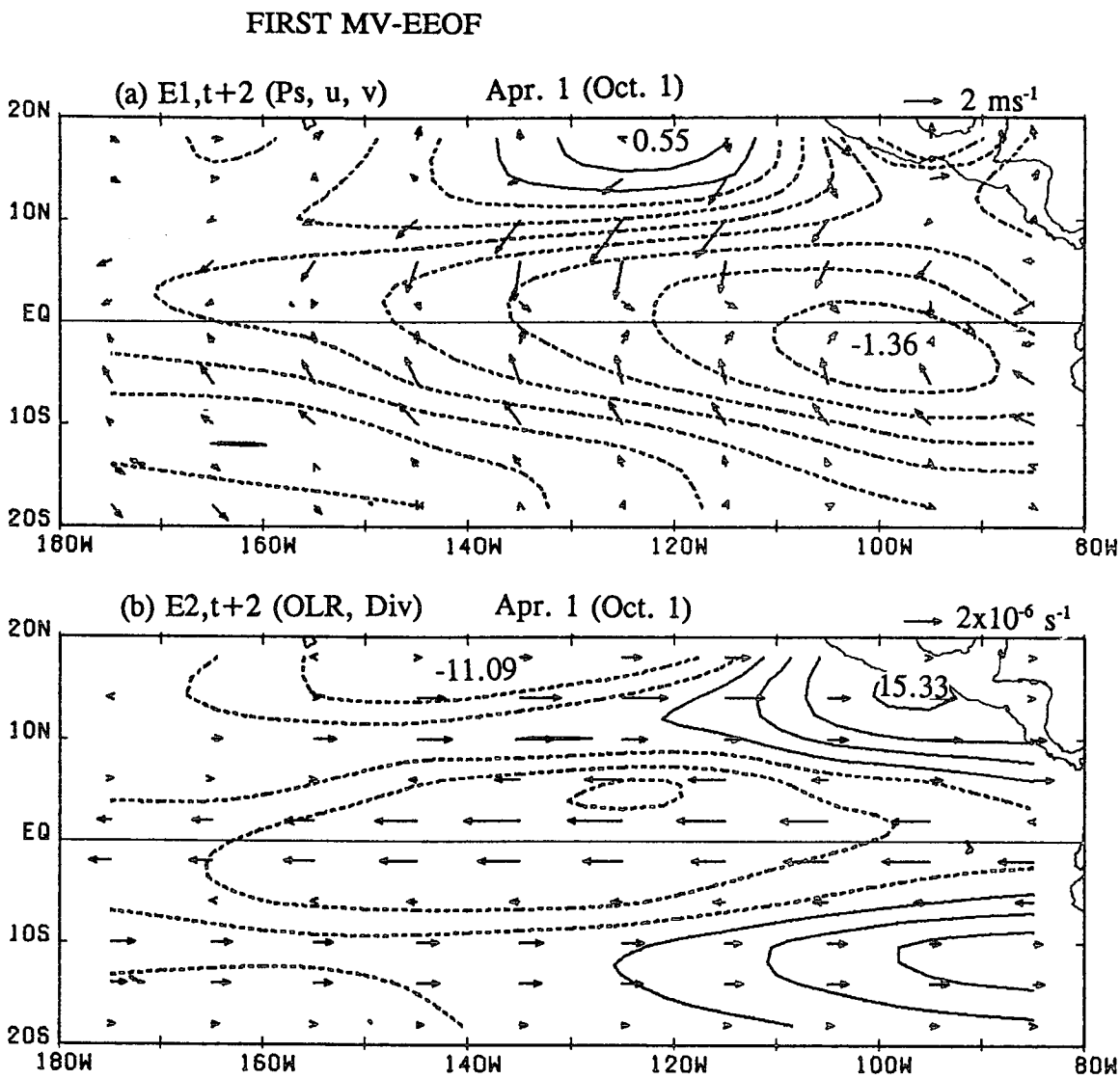

FIG. 6. The first MV-EEOF of the equatorial–coastal mode at $t + 2$ month for sea level pressure (contour interval 0.2 hPa) and surface winds (a), and OLR (contour interval 4 W m^{-2}) and surface wind divergence (b). Surface wind divergence is expressed by arrows in (c). Eastward (westward) arrows mean divergence (convergence).

1966; Horel 1982). It follows that this mode manifests itself as a result of atmosphere–ocean interaction.

6. Forced monsoonal mode

Figure 7 displays the annual cycle of the zonal-mean antisymmetric components of SST, SLP, surface winds, and OLR (hereafter referred to as zonal-mean antisymmetric mode). The amplitude of the annual cycle in SST increases with latitude from zero at the equator to 1.4°C at 20°N and 20°S. The meridional SST gradient reverses its sign twice a year with a maximum and a minimum occurring in September and March, respectively. Comparison of Fig. 7a with Fig. 1c indicates that the annual variation of the zonal-mean antisymmetric SST is a direct response to the antisymmetric solar radiational heating. In subtropics the dynamic processes do not affect SST significantly; thus, the warming of seawater lags the heating by about a quarter of a period (three months).

The annual cycle in zonal-mean antisymmetric SLP resembles that of SST. Changes in surface winds are in consonance with variations in the meridional pressure gradients. Between 20°S and 20°N the winds are directed down pressure gradients from the winter to summer hemisphere with maximum meridional winds crossing the equator. Due to the earth's rotation, the largest changes in zonal-mean westerlies (easterlies)

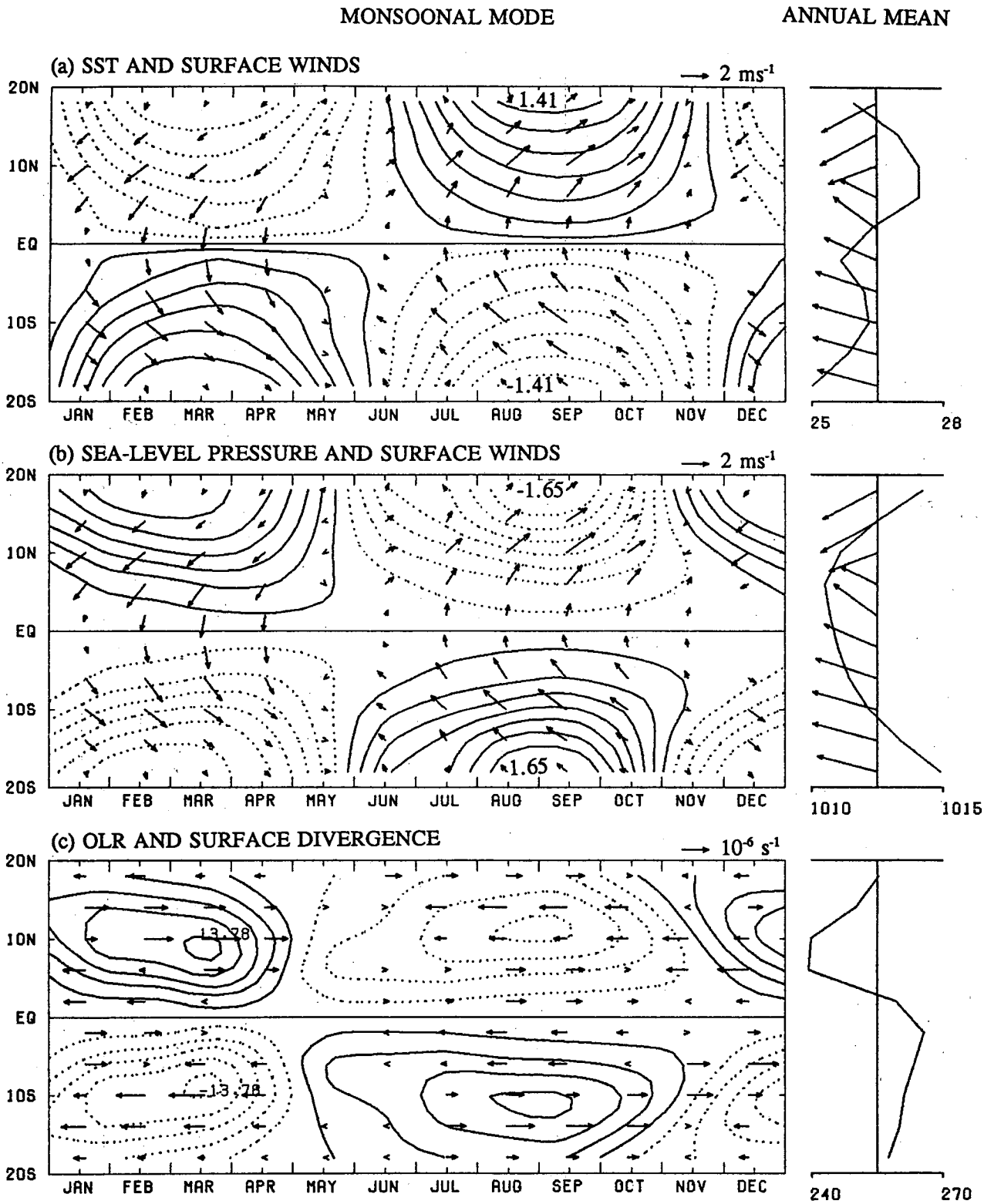

FIG. 7. The annual variation of the zonal-mean antisymmetric components in SST and surface winds (a), SLP and surface winds (b), and OLR and surface divergence (c). The curves and arrows in the right margins denote annual means of the corresponding total fields zonally averaged between 180° and 80°W. The contour intervals for SST, SLP, and OLR are 0.2°C, 0.2 hPa, and 3 W m^{-2}. No zero contour is shown. Surface wind divergence is expressed by arrows in (c). Eastward (westward) arrows mean divergence (convergence).

occur in the summer (winter) hemisphere between 5° and 15° latitude. This is a typical monsoon character. However, because the wind perturbation is substantially smaller than the annual mean winds (Fig. 7), the trades do not reverse their directions. The trades are strongest and closest to the equator during the late winter and early spring of the respective hemisphere (Wyrtki and Meyers 1976). Figure 7 demonstrates that the annual cycle of the trades is essentially an "invisible" monsoon. It is in this sense that the zonal-mean antisymmetric annual perturbation will be referred to as a *monsoonal mode.*

The zonal-mean surface divergence depends on the meridional derivative of meridional wind and is antisymmetric with respect to the equator (Fig. 7c). In March, the maximum convergence and cloudiness (minimum OLR) occur near 10°S, whereas the maximum divergence and OLR occur near 10°N. The former corresponds to the maximum cloudiness of the year in the southeast trades, and the latter reflects the weakening and southward shift of the intertropical convergence zone (ITCZ). As a result, the total amount of cloud and precipitation exhibits a hint of double ITCZ (Sadler 1969; Taylor 1973). During northern summer, the ascending branch (as implied by negative OLR) of the monsoonal mode appears at 12°N, implying an enhanced ITCZ.

An important feature of the monsoonal mode is the phase difference between SST and SLP/surface winds. Although the extreme phases in SST and SLP appear to occur nearly contemporaneously (around February–March and August–September), the transition phases (from winter to summer or vice versa) in SLP and surface winds lead those in SST (Fig. 7), suggesting the atmospheric variation is not a passive response to *local* ocean thermal condition. In fact, the response of the midlatitude atmosphere to the shift of the maximum insolation from one hemisphere to the other is more prompt than the tropical ocean because the amplitude of the insolational cycle is larger and the land effect is stronger in the midlatitudes. Therefore, in the Tropics the transition in atmospheric circulation leads that in SST. This phase leading has notable implication for understanding the annual cycle of SST in the tropical ocean (discussed in detail in section 7).

7. Interaction between the monsoonal and equatorial–coastal modes

The principal processes, which in theory can change SST, are net (shortwave and longwave) radiational flux and latent and sensible heat flux at the ocean surface, upwelling and turbulent mixing, and advection by ocean currents. Inspection of the Oberhuber (1988) atlas leads to the conclusion that the net radiational flux has little causal relation with the SST variation in the cold tongue region. In a recent heat budget study using mooring data near the equator along 110°W, Hayes et al. (1991) concluded that the annual cycle in SST cannot be explained by the annual cycle in insolation and surface heat fluxes. Wyrtki's (1981) heat budget study indicated that the South Equatorial Current contributes to the maintenance of the cold tongue, but the contribution of upwelling is much larger.

The interpretation of the weakening and reestablishment of the cold tongue presented in this section is based on the following hypothesis: The change of SST in the cold tongue is primarily caused by surface wind variation, which affects SST through changing ocean circulation (upwelling and advection), turbulent mixing, and surface latent heat flux.

a. The cause of the annual weakening of the cold tongue

September marks the extremely cold phase for the central cold tongue at locations C and E1 (Table 3 and Fig. 2c). Meanwhile, the monsoonal mode reaches its northern summer extreme condition: the southeast (northeast) trades are strongest (weakest). From October to November the southeast trades decline, whereas the northeast trades recover, both rapidly; the near-equatorial trough and associated convergence zone shift equatorward abruptly at a speed of 4° latitude per month (figure not shown). As a result, both the easterly wind along the equator and the alongshore wind off the coast of Peru decrease sharply as shown in Figs. 8a and 8b. The decline of the southeast trades has a twofold impact on SST. First, the decrease in wind speeds reduces evaporational latent heat loss of the ocean and favors warming of the cold tongue. Second, it suppresses equatorial and coastal upwelling and also favors the warm-up of the cold tongue. The coastal warming may effectively reduce the cold advection by the Peru and South Equatorial Currents, enhancing the equatorial warming. By November (December) the alongshore winds (equatorial easterlies) exceed their annual means. One month later in December (January), the coastal (equatorial) SST becomes higher than the annual mean (Figs. 8a and 8b). The further warm-

TABLE 3. Four phases of the annual cycle in SST at four locations shown in Fig. 2c: C (78°–82°W, 8°–14°S), E1 (96°–104°W, 2°N–2°S), E2 (122°–128°W, 2°N–2°S), and EC (80°–86°W, 2°N–2°S). Warming (cooling) means the transition from below (above) to above (below) the annual mean. Peak warm (cool) means the maximum (minimum) SST of the year.

Location	Peak cool	Warming	Peak warm	Cooling	Annual range (°C)
C	Sep	Dec	Mar	Jun	5
E1	Sep	Jan	Mar–Apr	Jun–Jul	5
E2	Oct	Jan–Feb	Apr	Jul	3
EC	Aug	Dec–Jan	Feb–Mar	Jun	2

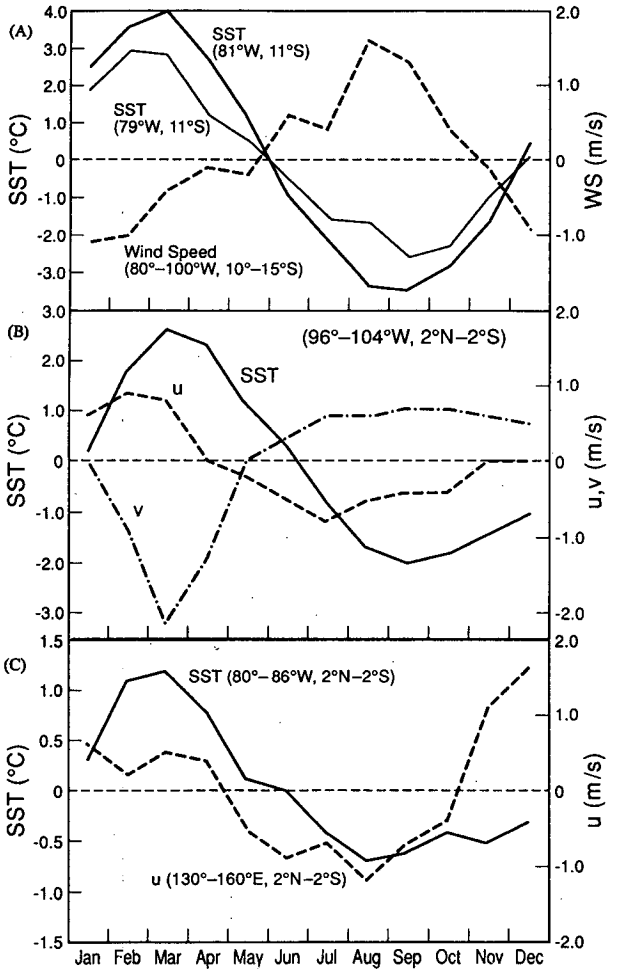

FIG. 8. Annual perturbations (departures of the climatological monthly means from the corresponding annual means) of (a) SST at 11°S, 81°W and 11°S, 79°W and the alongshore wind speed averaged over the area 10°–15°S, 80°–100°W; (b) SST and surface zonal (u) and meridional (v) wind speed averaged over the area 2°N–2°S; 96°–104°W; and (c) SST at location EC (2°N–2°S, 80°–86°W) and the surface zonal wind speed (u) averaged over the remote equatorial western Pacific (2°N–2°S, 130°–160°E).

up of the cold tongue is also partially attributed to the sustained weakening of the coastal southeast trades and equatorial easterlies, which reach their minimum strengths in January and February, respectively; both lead the corresponding coastal and equatorial peak warm seasons by one or two months (Figs. 8a and 8b, Table 3). The changes in cross-equatorial winds are nearly in phase with SST variation at locations E1 and E2 (Fig. 8b), suggesting that they may also play a role in equatorial warming via reducing evaporational latent heat loss.

Although the response of SST to changes in local wind forcing is commonly observed along the coast of Peru between 5° and 20°S and along the equator in the eastern Pacific, the annual warming occurring off the coast of Ecuador (location EC in Fig. 2c) is not related to the variations in local winds. Figure 8c shows, however, that the warming in January and the peak warm in February–March at EC lag, respectively, by about two months the onset (in November) and the peak (in December) phases of the westerly perturbation in the remote equatorial western Pacific. The remote forcing in the western Pacific may generate an annual downwelling Kelvin wave propagating eastward and affecting the annual variation of SST off the coast of Ecuador. Lukas (1981) found a remotely forced annual downwelling event from January to March along the equator near the eastern boundary. He suggested that the observations are consistent with the passage of an equatorial Kelvin wave from the equator to coastal region.

Another question related to the annual warming of the cold tongue is: Why does the maximum warming along the equator occur around 95°W? This depends mainly on two factors: the longitudinal distributions of the relaxation of easterly stress and the thermocline depth. The weakening of the equatorial easterlies occurring from December to March takes place mainly between 90° and 130°W with a maximum around 100°W (Philander and Chao 1991, Fig. 3). The thermocline depth has a minimum along the equator near 95°W (Meyers 1979, Fig. 3). It follows that the strongest warming along the equator should be most favorable around 95°–100°W where the thermocline is shallowest and the westerly perturbation is strongest.

b. The onset of the eastern North Pacific monsoon

Murakami et al. (1992) have shown that the triangle region in the eastern North Pacific, which is enclosed by the northern boundary of the equatorial cold tongue; the straight line between 5°N, 120°W and 20°N, 100°W; and the west coast of the Central America exhibit typical summer monsoon characteristics: Both the OLR and HRC indicate a concentrated summer rainfall and a large annual range; the surface winds reverse from winter northeasterlies to summer southwesterlies (the ITCZ changes from a trade wind convergence zone in winter to a monsoon trough in summer); and the upper-tropospheric winds change from winter westerlies to summer easterlies. Figure 9b shows that the annual variation of HRC (or precipitation) west of 120°W is quite different from that east of 120°W: the former has a lasting wet season with a peak in November, whereas the latter has a more concentrated wet season with a peak in July. The former is typical climate for a trade wind convergence zone, whereas the latter is typical summer monsoon climate (Wang 1994).

Mitchell and Wallace (1992) have speculated that the movement of the continental (Colombia and Panama) monsoon convection from the equatorial belt into the Northern Hemisphere extends westward into

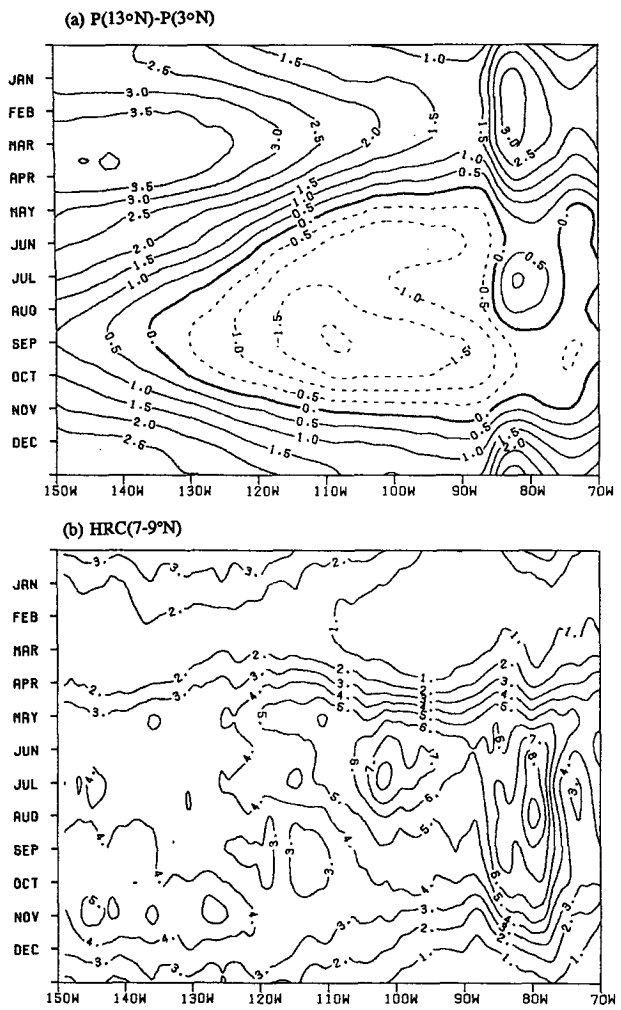

FIG. 9. Climatological monthly means of (a) SLP difference (hPa) between 13°N and 3°N, and (b) HRC (day/mo) averaged for the latitude belt between 7°N and 9°N in the eastern Pacific.

the warm pools along 9°N to form the oceanic ITCZ or induce the onset of the summer monsoon in May.

Figure 9 displays longitudinal variation of climatological monthly mean SLP gradients and HRC along 8°N. The reverse of the pressure gradients between 3°N and 13°N (implying a change from northeast wind to southwest wind near 8°N) starts earlier over the open ocean around 90°W than over the Central America (Fig. 9a). The onset of deep convection (as measured by monthly frequency of HRC higher than 4 days) shows no sign of phase lag between the east and west along the same latitude (Fig. 9b). Inspection of the meridional cross sections along 95° and 110°W (figure not shown) reveals that the swift northward shift of the ITCZ from April to June is more evident along 110°W than along 95°W. These observations suggest that the convective development and northward shift of the ITCZ over the eastern North Pacific in May is unlikely to be controlled by the northward movement of the continental monsoon over Columbia and Central America.

It is found, instead, that the evolution of the equatorial–coastal mode plays a critical role in the onset of the eastern North Pacific summer monsoon. March and April are the peak warm season for the central part of the cold tongue (Table 3). The annual decrease of SST along the equator first occurs off the coast of Ecuador in late March and early April. This is concurrent with the buildup of the warmest area around 100°W, which induces perturbation easterlies and upwelling off the coast of Ecuador. From April to May, the warming area associated with the equatorial–coastal mode spreads westward and poleward (Fig. 4). Concurrent equatorial cooling occurs east of 100°W. The simultaneous cooling at the equator and the warming at 10°–15°N reverses the signs of the meridional SST and SLP gradients. Figure 10 shows that along 95°W the SST difference between 10°N and 2°N ($T_{10} - T_2$), associated with the equatorial–coastal mode, changes dramatically from −0.5°C in April to 0.8°C in May, whereas the SST difference $T_{10} - T_2$, associated with the forced monsoonal mode, changes slightly from −0.6°C in April to −0.2°C in May. The sudden reversal of the meridional perturbation SST gradients from April to May is primarily due to the coupled equatorial–coastal mode rather than the forced monsoonal mode. A similar situation in reversal of meridional gradients happens in the perturbation SLP field. The rapid enhancement of the poleward SST and SLP gradients north of the cold tongue is attributed to the decay of the equatorial–coastal mode and plays a major role in the onset of the eastern North Pacific summer monsoon. This may also explain why the summer monsoon starts earlier over the ocean (around 100°W) than over Central America.

In addition to the influence of the equatorial cold tongue, the continental heating over Mexico, which generates a north–south oriented surface pressure trough along 100°W (see the atlas of Sadler et al. 1987), is another favorable factor. In fact, the surface pressure at Mexico City (approximately 20°N, 100°W) exhibits an annual minimum in May. The southward extension of this land-based pressure trough induces significant perturbation westerlies and southwesterlies to its south and favors the northward advance of the ITCZ and the onset of the summer monsoon.

From April to June, the establishment of the eastern North Pacific summer monsoon, in turn, intensifies southerlies between the cold tongue and the monsoon trough (or ITCZ). Mitchell and Wallace (1992) hypothesized that the intensifying southerlies along the northern fringe of the equatorial waveguide induces a remote response, bringing cold water to the surface just to the south of the equator, as in the numerical experiment of Philander and Pacanowski (1981), to intensify the equatorial cold tongue. The further re-

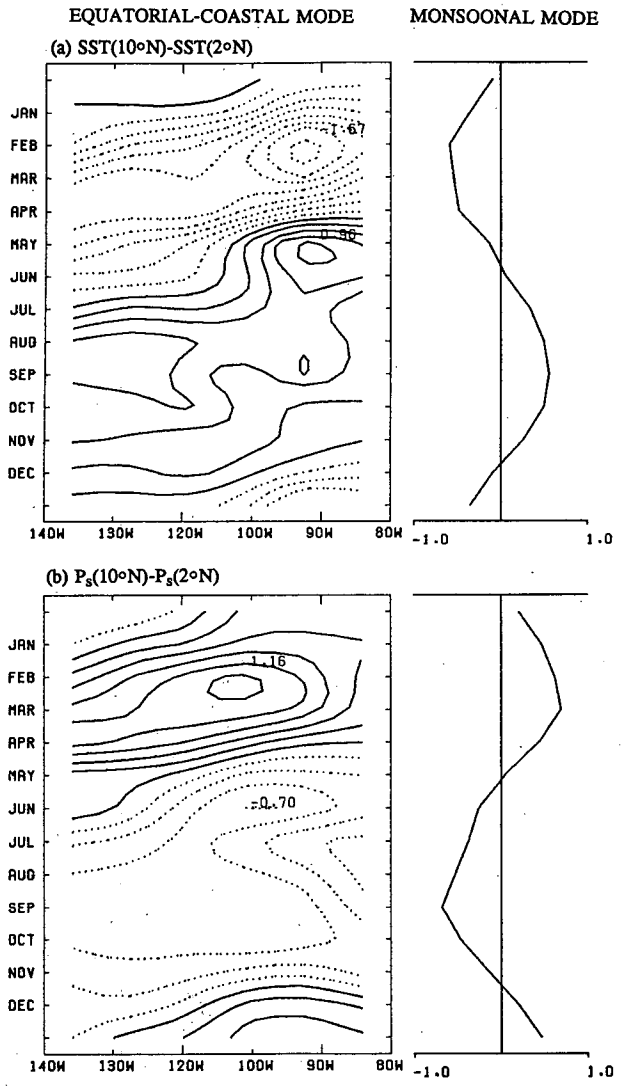

FIG. 10. The contour plot of the differences in SST (a) and surface pressure (b) between 10°N and 2°N associated with the coupled equatorial–coastal mode. The contour interval for SST and pressure are 0.2°C and 0.2 hPa. The right margins are the corresponding counterparts associated with the forced monsoonal mode.

establishment of the cold tongue from late May to August involves interaction between the southerlies and the meridional SST gradients. This interaction enhances both the cooling of equatorial water and the development of the southwest monsoon. Mitchell and Wallace (1992) also suggested that the continuous cooling in September and October after the decay of the monsoon results from the reduced solar radiation due to the shading of the stratocumulus deck formed over the cold water, but the cause of the formation of the stratocumulus clouds is unknown.

8. Summary and discussions

The annual perturbations (departures of climatological monthly means from the corresponding annual means) of SST, SLP, surface winds, and clouds as measured by OLR and HRC in the tropical eastern-central Pacific are partitioned into two modes: one asymmetric and one quasi-symmetric about the equator.

The asymmetric mode is an invisible monsoonal mode that has relatively large variance (due mainly to the contrast between the Northern and Southern Hemispheres) occurring in January–March and July–October. The amplitudes of this mode in SST and SLP increase with latitude. It is forced by the differential insolation between the Northern and Southern Hemispheres. It represents the tropical part of a global response of the atmosphere–ocean–land system to external solar forcing. The surface wind variation of the monsoonal mode leads that of SST in early summer and early winter, suggesting that the transition of SST from cold to warm, or vice versa, is partially caused by the changes in the trade winds.

The quasi-symmetric mode is an equatorial–coastal mode that has relatively large variance (due mainly to the contrast between the equator and midlatitudes) occurring in April–June and November–December. This mode has maximum amplitudes of SST and SLP occurring on the equator and near the South American coast. It exhibits a distinctive annual cycle with a wet and warm season in March–April and a dry and cold season in September–October. This mode has little to do with the annual march in insolation. The latter on the equator is forced by the semiannual cycle in solar declination and a minor annual cycle in earth–sun distance. The coherent structure and evolution between SST and atmospheric boundary layer circulation indicate that this mode results from large-scale air–sea interaction. The development of this mode is characterized by simultaneous spatial expansion and intensification with the maximum warming staying around 4°S, 95°W where the oceanic thermocline depth is a minimum. The westward propagation is a manifestation of the interaction between the Walker circulation and SST (Horel 1982), whereas the poleward (mainly northward due to the proximity of the Central–North American landmass to the ocean) propagation is speculated to be a result of suppression of poleward Ekman transport of upwelled cold water and the dispersion of the warming area by reflected Rossby waves. This process is possibly enhanced by spring warming of the landmass over Mexico and by reduced evaporational latent heat loss.

It is the evolution of the equatorial–coastal mode that forms a distinct equatorial regime of annual cycle in the tropical oceans of the Western Hemisphere (the eastern Pacific and Atlantic Oceans). In sharp contrast, the forced antisymmetric monsoonal mode dominates the annual variation of the tropical oceans in the Eastern Hemisphere (the Indian and western Pacific Oceans). The peculiar annual cycle in the eastern Pacific originates from the coupling of the atmosphere

and ocean. This is reflected in the fact that the changes in the northeast and southeast trades affect equatorial and coastal upwelling and surface latent heat flux; on the other hand, the decay of the equatorial mode (equatorial cooling and off-equatorial warming) influences the onset of the eastern North Pacific summer monsoon. The interplay between the two modes and the two media are also exemplified by the development of cold tongue–monsoon (or ITCZ) complex during northern summer as described by Mitchell and Wallace (1992) and Murakami et al. (1992).

The existence of a cold tongue is the result of complex atmosphere–ocean–continent interaction. On the one hand, the SST distribution, in particular the thermal contrast between the cold tongues and warm pools, is a principal geophysical factor that determines the climatic locations of the ITCZ and South Pacific convergence zone (SPCZ) (Wang and Li 1993). The convective heating released in these convergence zones along with the SST gradient-induced pressure gradient force in the boundary layer drives the Pacific trades. On the other hand, the oceanic Ekman-layer divergence, induced by the equatorial easterly stress and alongshore wind stress of the trades, produces equatorial and coastal upwelling, which maintains the cold tongue and associated oceanic thermal contrasts. The influence of the air–sea interaction on the free tropospheric circulation is, however, restrained by the stable atmospheric stratification. The coherency in the annual variations between the 850-hPa equatorial zonal wind and SST is considerably weaker than that between the surface zonal wind and SST (figure not shown). The variation of 200-hPa equatorial zonal wind is independent of SST and is primarily controlled by the midlatitude conditions (Murakami and Wang 1993).

The present analysis is focused on the annual perturbation, which is the departure of the climatological monthly mean from annual means. The analysis procedure is valid up to the limit where the nonlinear transient effects are small. The analysis of annual perturbation alone is based on the assumption that the physical processes responsible for the maintenance of the annual-mean state are different from those governing the annual perturbation. The annual-mean fields are highly asymmetric with regard to the equator. The important question of how the annual-mean states form remains to be addressed. In addition, there are several issues that require further investigations, including the nature of unstable development of the equatorial–coastal mode, the relative importance of surface net heat flux versus surface wind forcing in the SST variation in the eastern Pacific, the relative importance of the continental heating over Mexico and the SST gradients north of the cold tongue in the onset of the eastern North Pacific summer monsoon, and the relative importance of the equatorial zonal versus meridional wind forcing in the annual cycle of the Pacific cold tongue. The role of the antisymmetric mode in triggering and promoting annual warming of the cold tongue may have an implication for the ENSO cycle. This, however, needs to be studied by careful analysis of long-term records.

Acknowledgments. This work was initiated during the workshop lead by George Philander at Princeton University. The author wishes to thank T. Mitchell, G. Philander, T. Murakami, P. Chang, and K. Wyrtki for their stimulating discussions and insightful comments on an early version of the manuscript. The comments by anonymous reviewers which led to a significant improvement of the paper are appreciated. The author thanks J. M. Oberhuber for providing surface heat flux data and T. Li, J. Huang, and Z. Tang for their computational and graphical assistance. This work is supported by Equatorial Pacific Ocean Climate Study and Tropical Ocean Global Atmosphere programs of NOAA.

REFERENCES

Bjerknes, J., 1966: A possible response of the atmospheric Hadley circulation to equatorial anomalies of ocean temperature. *Tellus,* **18,** 820–829.

——, 1969: Atmospheric teleconnections from the equatorial Pacific. *Mon. Wea. Rev.,* **97,** 526–535.

Budyko, M. I., and D. H. Miller, 1974: *Climate and Life.* Academic Press, 508 pp.

Garcia, O. S., 1985: *Atlas of Highly Reflective Clouds for the Global Tropics: 1971–1983.* U.S. Department of Commerce, National Oceanic and Atmospheric Administration. Environmental Research Laboratories, 365 pp.

Gruber, A., and A. F. Krueger, 1984: The status of the NOAA outgoing longwave radiation data set. *Bull. Amer. Meteor. Soc.,* **65,** 958–962.

Hayes, S. P., P. Chang, and M. J. McPhaden, 1991: Variability in sea surface temperature in the eastern equatorial Pacific. *J. Geophys. Res.,* **96,** 10 553–10 566.

Hastenrath, S., and P. Lamb, 1977: *Climate Atlas of the Tropical Atlantic and Eastern Pacific Ocean.* University of Wisconsin Press, 122 pp.

——, and ——, 1978: On the dynamics and climatology of surface flow over the eastern oceans. *Tellus,* **30,** 436–448.

Horel, J. D., 1982: On the annual cycle of the tropical Pacific atmosphere and ocean. *Mon. Wea. Rev.,* **110,** 1863–1878.

Janowiak, J. E., A. F. Krueger, P. A. Arkin, and A. Gruber, 1985: *Atlas of Outgoing Longwave Radiation Derived from NOAA Satellite Data.* NOAA Atlas No. 6, U.S. Department of Commerce, 44 pp.

Lindzen, R. S., and S. Nigam, 1987: On the role of the surface temperature gradient in forcing low level winds and convergence in the tropics. *J. Atmos. Sci.,* **44,** 2440–2458.

Lukas, R., 1981: The termination of the equatorial undercurrent in the eastern Pacific. Ph.D. dissertation, University of Hawaii at Manoa, 127 pp.

Meyers, G., 1979: Annual variation in the slope of the 14°C isotherm along the equator in the Pacific Ocean. *J. Phys. Oceanogr.,* **9,** 885–891.

Mitchell, T. P., and J. M. Wallace, 1992: On the annual cycle in equatorial convection and sea-surface temperature. *J. Climate,* **5,** 1140–1156.

Morrissey, M. L., 1986: A statistic analysis of the relationship among rainfall, outgoing longwave radiation and the moisture budget during January–March 1979. *Mon. Wea. Rev.,* **114,** 931–942.

Murakami, T., and B. Wang, 1993: Annual cycle of the equatorial east–west circulation over the Indian and Pacific Oceans. *J. Climate,* **6,** 932–952.

——, ——, and S. W. Lyons, 1992: Summer monsoons over the Bay of Bengal and the eastern North Pacific. *J. Meteor. Soc. Japan,* **70,** 191–210.

Oberhuber, J. M., 1988: An atlas based on the "COADS" data set: The budget of heat, buoyancy and turbulent kinetic energy at the surface of the global ocean. Max-Planck-Institut fur Meteorologie Rep. No. 15, 196 pp.

Philander, S. G. H., and R. C. Pacanowski, 1981: The oceanic response to cross-equatorial winds (with application to coastal upwelling in low latitude). *Tellus,* **33,** 201–210.

——, and Y. Chao, 1991: On the contrast between the seasonal cycles of the equatorial Atlantic and Pacific Oceans. *J. Phys. Oceanogr.,* **21,** 1399–1406.

Sadler, J. C., 1969: *Average Cloudiness in the Tropics from Satellite Observation.* East–West Center Press, 22 pp. and 12 plates.

——, M. A. Lander, A. M. Hori, and L. K. Oda, 1987: *Tropical Marine Climatic Atlas. Vol. 1: Pacific Ocean.* Report UHMET 87-02, Department of Meteorology, University of Hawaii, 27 pp.

Taylor, R. C., 1973: *An Atlas of Pacific Islands Rainfall.* Tech. Rep. HIG-73-9 (Data Rep. No. 25), Hawaii Institute of Geophysics, University of Hawaii, 175 pp.

Wang, B., 1992: The vertical structure and development of the ENSO anomaly mode during 1979–89. *J. Atmos. Sci.,* **49,** 698–712.

——, 1994: Climatic regimes of tropical convection and rainfall. *J. Climate,* **7,** 1109–1118.

——, and T. Li, 1993: A simple tropical atmosphere model of relevance to short-term climate variations. *J. Atmos. Sci.,* **50,** 260–284.

Weare, B. C., and J. S. Nasstrom, 1982: Examples of extended empirical orthogonal function analyses. *Mon. Wea. Rev.,* **110,** 481–485.

——, P. T. Strub, and M. D. Samuel, 1980: *Marine Climate Atlas of the Tropical Pacific Ocean.* Dept. of Land, Air and Resources, University of California, Davis, 147 pp.

Wyrtki, K., 1965: The annual and semiannual variation of SST in the North Pacific Ocean. *Limnol. Oceanogr.,* **10,** 307–313.

——, 1981: An estimate of equatorial upwelling in the Pacific. *J. Phys. Oceanogr.,* **11,** 1205–1214.

——, and G. Meyers, 1975: The trade wind field over the Pacific Ocean. Part I: The mean field and the mean annual variation. Rep. No. HIG-75-1, Hawaii Institute of Geophysics, University of Hawaii, 26 pp.

——, and ——, 1976: The trade wind field over the Pacific Ocean. *J. Appl. Meteor.,* **15,** 698–704.